JOURNAL OF SOLID STATE CHEMISTRY 8, 242–252 (1973)

The Optical Properties of Some Alkali Metal Tungsten Bronzes from 0.1 to 38 eV

D. W. LYNCH, R. ROSEI, J. H. WEAVER, AND C. G. OLSON

Ames Laboratory-USAEC and Department of Physics, Iowa State University, Ames, Iowa 50010

Received February 23, 1973

The optical properties of the alkali metal tungsten bronzes are investigated. A review of existing data and the interpretation thereof is presented. Our absorptivity or reflectivity data for two cubic Na bronzes and for a tetragonal K bronze in the energy range 0.1 to 38 eV are displayed; the data are Kramers-Kronig analyzed and the optical constants are obtained. When feasible, comparisons are made with the existing data for the bronzes as well as for ReO_3, which is structurally similar. The interpretation of optical constants is based on an existing band structure for ReO_3 and modifications thereto are suggested.

Introduction

The tungsten bronzes, M_xWO_3, where M is a monovalent metal (Na or K for our purposes) and $0 < x \lesssim 1$, display a variety of physical properties which depend on x. For $x = 0$, the material is an insulator, WO_3. For low x, the bronzes are orthorhombic or tetragonal semiconductors (*1*). For intermediate x values they are hexagonal or tetragonal metals (*2*). For $0.48 \lesssim x < 0.93$, Na_xWO_3 is a cubic (perovskite structure) metal; K_xWO_3 is metallic and hexagonal in the range $0.23 \gtrsim x \gtrsim 0.33$ and tetragonal for $0.33 < x < 0.75$ (*2*). The colors of the bronzes, from whence the name "bronze" derives, vary strikingly with x. Since knowledge of the optical properties of solids has in the past led to a better understanding of electronic structures, it is natural to examine the bronzes. In the following we review previous optical measurements on the cubic sodium tungsten bronzes. Then we discuss our measurements of the optical absorptivity or reflectivity of single crystals of cubic Na_xWO_3 ($x = 0.65$ and 0.735) and tetragonal K_xWO_3 ($x = 0.63$) in the energy range 0.1 to 38 eV. The latter are the first optical measurements on noncubic bronzes.

The first published optical measurements dealing with the bronzes were of the diffuse reflectivity of compressed, powdered sodium bronzes by Brown and Banks (*4*). The x-dependence of the position of the major reflectivity minimum near 2.3 eV cannot be interpreted reliably since the measured reflectivity represents an average over a wide range of angles of incidence; such spectra are not amendable to the usual Kramers-Kronig analysis of specular reflectance. In general, reflectance spectra are difficult to interpret since the measured quantity results from an interplay of the real and the imaginary parts of the complex refractive index $\tilde{N}$ or complex dielectric constant $\tilde{\varepsilon}$ (*5*):

$$\tilde{N} = n + ik, \tag{1}$$

$$\tilde{\varepsilon} = \varepsilon_1 + i\varepsilon_2 = \tilde{N}^2. \tag{2}$$

The complex amplitude reflection coefficient at normal incidence is

$$\tilde{r} = \frac{\tilde{N} - 1}{\tilde{N} + 1}, \tag{3}$$

and

$$R = \frac{(n-1)^2 + k^2}{(n+1)^2 + k^2} = |\tilde{r}|^2, \tag{4}$$

where R is the normal-incidence *specular* reflectivity. A sharp drop in R could arise if $k \approx n$ with $n, k < 1$, $dn/d\lambda < 0$ and $dk/d\lambda > 0$ (or $\varepsilon_2 \ll 1$, and ε_1 rises through 0) which is characteristic of a

plasma resonance and is accompanied by relatively slight absorption. This is in contrast to an optical absorption peak which is often assumed to be responsible for a dip in R. Thus, while the positions of the dip in R as measured by Brown and Banks (*4*) vary with x, it does not seem fruitful to try to correlate their data with models for the electronic structure; $\tilde{\varepsilon}$ spectra should be used for that.

The pioneering work by Brown and Banks was followed by investigations of Na bronzes by Dorothy and Lynch (*6*) and by Feinleib and Scouler (*7*). The former used the method of Avery (*8*) to obtain $\tilde{N}$, using polished, etched single crystals. The latter made normal-incidence reflectivity measurements on polished, unetched single crystals, from which $\tilde{N}$ could be obtained by Kramers-Kronig analysis. Lynch and Dorothy used their $\tilde{N}$ data to calculate R spectra. Their infrared reflectivity values were considerably higher than those reported for compressed powders, but were lower than those of Feinleib and Scouler. The discrepancy probably arose from a systematic error in the measurements of the former due to a possible layer of WO_3 on the surface of the crystals. In the infrared, such a dielectric film produces smaller errors in the reflectivity measured at near-normal incidence than in the quantities measured by the method of Avery, i.e., the ratios of the reflectivities for s- and p-polarization at several angles of incidence, including at least one large angle.

Dickens, Quilliam and Whittingham (*9*) measured the diffuse reflectivity of compressed powdered samples using both pure bronzes and bronzes mixed with powdered MgO and KCl before compacting. Their results for undiluted powders agreed qualitatively with those of Brown and Banks. Taylor (*10*) used a similar technique but with different results. Fujieda (*11*) used the method of Avery to determine $\tilde{N}$ for compressed powders of Na- and K-bronzes. To test her technique, she performed similar measurements with organic dyes of known optical properties. The reflectivity spectra computed from her $\tilde{N}$ spectra fell well below those computed for, or measured on, single crystals.

Consadori and Stella (*12*) measured the near normal-incidence reflectivity of polished, etched cubic Na_xWO_3 ($x = 0.517$ and 0.72) in the energy range 1.76 to 6.0 eV at room temperature. These measurements were followed by electroreflectance measurements (*13*). The reflectivity spectra generally agree with those of Feinleib and Scouler (*7*) with the exception of a dip in R at about 5 eV which the latter did not see. Consadori and Stella observed a time-dependence in the reflectivity spectra, as though a film were growing on the surface. Such a film should be (reasonably) transparent from near the reststrahl region of WO_3 to the absorption edge of WO_3 (2.6 to 3.0 eV) (*14*). While it should not severely alter R in the near infrared, it could produce large errors in the method of Avery. The effects could also be important in any measurements on powders where a larger fraction of the sample is surface and where reflection at large angles of incidence contributes to the spectra. It seems reasonable to place more confidence in normal-incidence reflectivity spectra than in any of the others.

The interpretation of the spectra given by Consadori and Stella seems to be generally correct and we summarize it here. Although they did not Kramers-Kronig analyze their spectra, the Na_xWO_3 reflectivity spectra were similar to that of ReO_3 which was analyzed by Feinleib, Scouler, and Ferretti (*15*) to give $\tilde{\varepsilon}$. This similarity is expected because the band structures of ReO_3 and Na_xWO_3 are thought to be similar. The WO_3 conduction band is composed roughly of a mixture of W $5d\ t_{2g}$ and O $2p\ \pi$ orbitals (*16*). The Na atoms act as donors and partly fill this band while not having a major effect on its form. The extent to which the corresponding picture of Re $5d\ t_{2g}$ and O $2p\ \pi$ orbitals for the ReO_3 conduction band is valid was discussed by Mattheiss (*17*).

The infrared optical behavior of metallic Na_xWO_3 is that of a free electron gas embedded in a dielectric medium. A free electron gas has a frequency-dependent dielectric constant given by

$$\tilde{\varepsilon}(\omega) = 1 - \omega_p^2/\omega(\omega - i/\tau), \qquad (5)$$

where τ is a relaxation time and the plasma frequency, ω_p, is given by $\omega_p^2 = 4\pi Ne^2/m^*$, there being N electrons of effective mass m^* per unit volume. Interband transitions presumably begin in the visible region (*12*), but the dispersion associated with the interband absorption contributes a real part ε_1^b to the infrared dielectric constant. This can be viewed as the polarization of the atomic cores and valence electrons. At low energies ε_1^b is constant, but varies with energy as the interband absorption edge is approached. The infrared optical properties are then described by

$$\tilde{\varepsilon} = \varepsilon_1^b + 1 - \omega_p^2/\omega(\omega - i/\tau). \qquad (6)$$

When inserted in Eqs. (1)–(4) this yields a high reflectivity for low photon energies, and a sharp drop in reflectivity at the "screened" plasma frequency ω_p' given by the solution of

$$\omega_p'^2 = \omega_p^2/[1 + \varepsilon_1^b(\omega_p')]. \quad (7)$$

The $\tilde{\varepsilon}$ of Eq. (6) then requires that R be small for $\omega > \omega'$, but interband transitions cause R to rise at higher ω. This effect is not included in Eq. (6) but must be added to it. For Na_xWO_3 ($x = 1$), $\hbar\omega_p = 5.0$ eV, while the reflectivity minimum is near 2.2 eV. Thus $\varepsilon_1^b(\omega_p')$ is roughly 4. Moreover, $\omega_p^2 \propto N/m^*$ so that for the cubic bronzes, $\omega_p \propto x^{1/2}$ if m^* is assumed independent of x. [The lattice parameter varies only slightly with x- (*18–20*).] Since the energy of the reflectivity minimum does *not* vary (*4*) as $x^{1/2}$, $\varepsilon_1^b(\omega_p')$ must vary with x. This is expected, for the absorption edge moves toward higher energy as x increases (see below) and ω_p' is fairly close to the edge, in a region where $\varepsilon_1^b(\omega)$ is not constant. Thus, the x-dependence of the position of the reflectivity minimum is the result of the interplay of the x-dependence of the free carrier parameters and of the change in the interband absorption with x. It is not necessary to invoke interference effects (*9*).

The interband absorption begins at an energy above that of the minimum in R. The initial rise in R is due to an increasing ε_1^b, before ε_2^b begins to rise above zero at the interband edge. Consadori and Stella (*12*) suggested that a change in slope at 3.10 eV may be the onset of interband absorption. This is close to the energy of the edge (*14*) in WO_3, whose band structure should be similar to that of cubic Na_xWO_3, despite the lower symmetry. There interband transitions presumably are from the top of the valence band, across the energy gap, to states at the Fermi level. The energy of such transitions should increase as x does, for the Fermi level rises, but it should not vary as $x^{2/3}$, the dependence expected for a free-electron conduction band. Electro-reflectance measurements (*13*) supported the view of Consadori and Stella that the interband optical absorption in Na_xWO_3 was similar to that in $BaTiO_3$ and $SrTiO_3$, crystals with band structures expected to be similar to that of cubic Na_xWO_3.

Since the Fermi level is expected to lie within a region containing several closely spaced bands derived from W 5*d*- and O 2*p*-functions, low energy interband transitions might be expected, but perhaps with low intensity because of small electric dipole matrix elements due to symmetry or a small joint density of states. Indeed, Matthiess showed that such transitions are expected in ReO_3 (*21*) and such transitions have been found experimentally (*22*).

Experimental Technique

The measured quantity was the reflectivity R, or the absorptivity, $A = 1 - R_1$ both at an angle of incidence of 10°. In the infrared, the visible and near ultraviolet (0.1 to 4.5 eV), a calorimetric technique was used and the absorptivity was measured at 4.2 K. The technique and apparatus have been described elsewhere in detail (*23*). In the vacuum ultraviolet from 5 to 38 eV, synchrotron radiation from the 240 MeV electron storage ring of the University of Wisconsin Physical Science Laboratory was used. The room temperature reflectivity data were obtained in this way in increments of 2.5 Å over the wavelength range 2500 to 310 Å. The technique will be described in detail in a subsequent paper (*24*). To provide a region of overlap for data from the calorimeter and the storage ring, a Cary Model 14R spectrophotometer was used with a reflectance attachment (*25*), and the room temperature reflectivity was determined in the range from 0.7 to 6 eV. The accuracy of the data obtained with the three instruments is estimated to be: $A = \pm 1\%$ at 1 eV for the calorimeter, $R = \pm 3\%$ for the storage ring, and $\pm 7\%$ for the Cary. The data obtained with the latter were accordingly adjusted to match the other more sensitive instruments in the regions of overlap. Thus our data cover the broad energy range from 0.1 to 38 eV.

Samples of Na and K bronzes have been studied with x values of 0.65 and 0.735 for Na_xWO_3 and 0.63 for K_xWO_3. The Na bronze sample with the higher x value was not studied in the vacuum ultraviolet (vuv). The Na bronzes were cubic and it was not necessary to polarize the radiation. For the tetragonal K bronze, a AgCl pile-of-plates polarizer was used in the energy range 0.1 to 0.7 eV. A Glan prism was used above 0.7 eV for the calorimeter and in the entire range of the spectrophotometer. For the vuv, use was made of the natural polarization (*26*) of synchrotron radiation; the sample itself was rotated appropriately. The data presented are labeled according to whether the electric field vector **E** was parallel to the $\hat{a}$ or the $\hat{c}$ axis for the tetragonal crystal.

The samples were grown by electrolysis (*27*). The K_xWO_3 sample was oriented with the $\hat{a}$–$\hat{c}$ plane in the surface, allowing measurement on a single face with both polarizations. The $Na_{.735}WO_3$ sample was grown with a (110) face. All samples had surface dimensions of at least 6×12 mm and typically were more than 2 mm in thickness. The samples were brittle but it was possible to cut them with a spark cutter at low power. Conventional polishing techniques were used and the resultant surfaces were very smooth, the final polishing abrasive being 0.05 μm diameter alumina paste. Immediately prior to loading a sample in any sample chamber, it was etched in a boiling solution of HNO_3:HCl (5:1 by volume) for at least 5 min. It was then washed in hot methanol and dried in a N_2 stream. For calorimeter and vuv measurements, it was quickly transferred to the respective vacuum chamber; the vacuum was typically 10^{-4} Torr within 15 min from the time of removal from the etch. It has been found that the infrared and visible absorptivity data obtained with a sample prepared in this manner were practically identical to those found using the same sample after it had been exposed to the atmosphere (but washed in methanol) for about 6 mo. Thus, if a surface film does form, it does so very quickly or is affected by the hot methanol solution. It is possible that it forms quickly but, as in the case of Al_2O_3, is of limited thickness. Unfortunately, since the nature or existence of the film is not known, it is impossible to take its optical properties into account when analyzing the data, as was done for example for a Cd crystal with a layer of CdO on the surface (24).

Results

The absorptivities of the two samples of Na_xWO_3 are shown in Fig. 1. The data were taken with the calorimeter at 4.2 K, and near-normal incidence. The absorptivity was measured for $x = 0.735$ only up to 4.5 eV. The low energy limit was 0.10 eV. It is seen from that the two curves effectively merge below 1.2 eV and that no structure is evident in the infrared. The dominant feature in each curve is the sharp rise in A. The peak values occur at 2.30 and 2.47 eV for $x = 0.65$ and 0.735, respectively; the maximum absorptivity is 0.986 for $x = 0.65$ and 0.994 for $x = 0.735$. It is clear from Fig. 1 that the absorptivity is practically independent of x in the infrared below 1.2 eV; the only difference we have observed between the two samples is in the position of the major absorption peak. It can be seen that an increase in Na concentration shifts the peak to higher energy. A corresponding change in color of the sample is observed visually, the lower x value corresponding to a purple while the higher value corresponds to an orange. This dependence of the peak position with x and the general features of the spectra are in good agreement with the results of Consadori and Stella (*12*) in the range 1.75 to 4.0 eV. While Consadori and Stella report a shoulder in A at

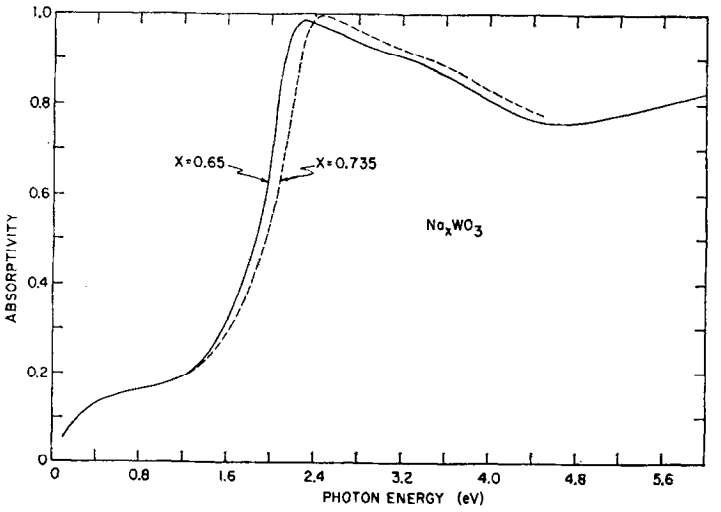

FIG. 1. Absorptivity of two cubic sodium tungsten bronzes at 4.2 K.

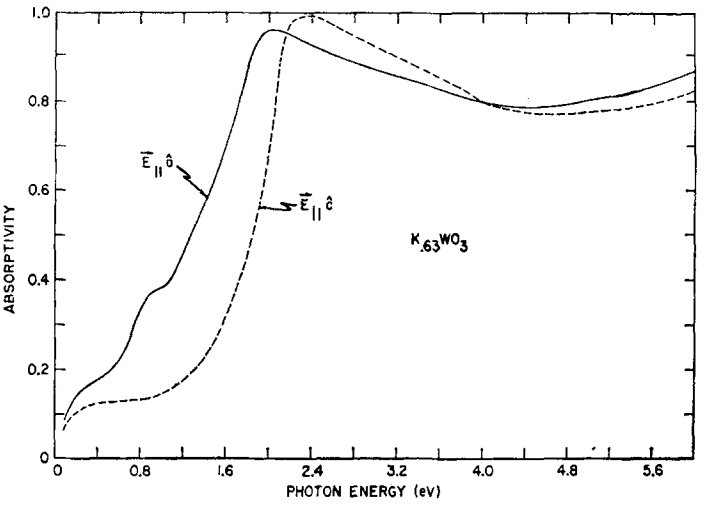

FIG. 2. Absorptivity of tetragonal $K_{.63}WO_3$ at 4.2 K for $\mathbf{E}_{\parallel}\hat{a}$ and $\mathbf{E}_{\parallel}\hat{c}$.

about 5 eV, we have observed no such feature. Likewise, the unpublished results of Scouler and Feinleib (7) show no structure in that region and are in agreement with our results.

A feature common to both samples was the slight shoulder on the high energy side of the principal peak, occurring at roughly 3.5 and 3.6 eV. The appearance of this structure was noted by Consadori and Stella who attributed it to the onset of interband transitions. More is said about this below.

The absorptivities for $\mathbf{E}_{\parallel}\hat{a}$ and $\mathbf{E}_{\parallel}\hat{c}$ for $K_{.63}WO_3$ are shown to 6 eV in Fig. 2. As was the case for the Na bronzes, the large peak in A is prominent, but equally dramatic is the anisotropy in the infrared. The results for $\mathbf{E}_{\parallel}\hat{c}$ are quite similar to those for the Na bronzes, but the structure apparent for $\mathbf{E}_{\parallel}\hat{a}$ at about 0.9 eV is new; it suggests the existence of low energy interband transitions which are allowed for $\mathbf{E}_{\parallel}\hat{a}$ but forbidden by selection rules or band structure for $\mathbf{E}_{\parallel}\hat{c}$, as well as for the cubic Na bronzes. The $\mathbf{E}_{\parallel}\hat{a}$ and $\mathbf{E}_{\parallel}\hat{c}$ curves also display the shoulder at about 3.5 eV which was noted for the other samples and was identified as the onset of interband effects. Clearly, for $\mathbf{E}_{\parallel}\hat{a}$ the onset occurs at considerably lower energy. We note also from Fig. 2 that the maximum in the peak in A occurs at 2.06 eV for $\mathbf{E}_{\parallel}\hat{a}$ and at 2.36 eV for $\mathbf{E}_{\parallel}\hat{c}$. Indeed, samples of the tetragonal bronze cut to expose separately planes normal to $\hat{a}$ and to $\hat{c}$ display different colors.

In the infrared, if $\omega\tau \gg 1$ and $\omega \ll \omega_p$, Eqs. (1)–(5) give $A = 2/\omega_p\tau$ for a free electron gas. Thus A is a small, energy-independent quantity. For th bronzes τ is not large enough for the inequalitie to hold, so A is expected to rise very slowly witl increasing energy. Such a rise is calculated to b much smaller than those observed in Figs. 1 and 2 if we calculate τ from dc resistivity data at 4.2 K Thus the structureless rise in A with increasing energy is a sign of low energy interband absorption.

The reflectivities for $Na_{.65}WO_3$ and the two polarizations of $K_{.63}WO_3$ are shown in Fig. 3 from 0.1 to 38 eV. For the sake of clarity, the former curve is shifted vertically and the abscissa at the right of Fig. 3 refers to it. The similarities of Na_xWO_3 and $\mathbf{E}_{\parallel}\hat{c}$ are quite clear. Neither has structure in the infrared, both have a sharp reflectivity minimum at 2.35 eV, and both have a shoulder at about 3.5 eV (this is more evident in Fig. 2 for $\mathbf{E}_{\parallel}\hat{c}$). The large broad reflectivity peak at 4.7 eV then gives way to a stepping rise between 8 and 12 eV. These latter features are also shared by $\mathbf{E}_{\parallel}\hat{a}$ though they appear to be shifted to lower energy by about 0.4 eV. Above about 13.5 eV, the two reflectivity curves for the $K_{.63}WO_3$ merge, to within the uncertainty of the data. Both then display weak, narrow structure in R at 18.5 and 21 eV and broader features at about 25 and 28.5 eV. Beyond 30 eV, the reflectivity drops smoothly to 0.0168 at 38 eV. Comparison with the Na bronze results shows that above 13 eV the K- and Na bronze have little in common. The $Na_{.65}WO_3$ has a broad shoulder at 15 eV while the K bronze has at most a slight hump at 14 eV. This is also true for the

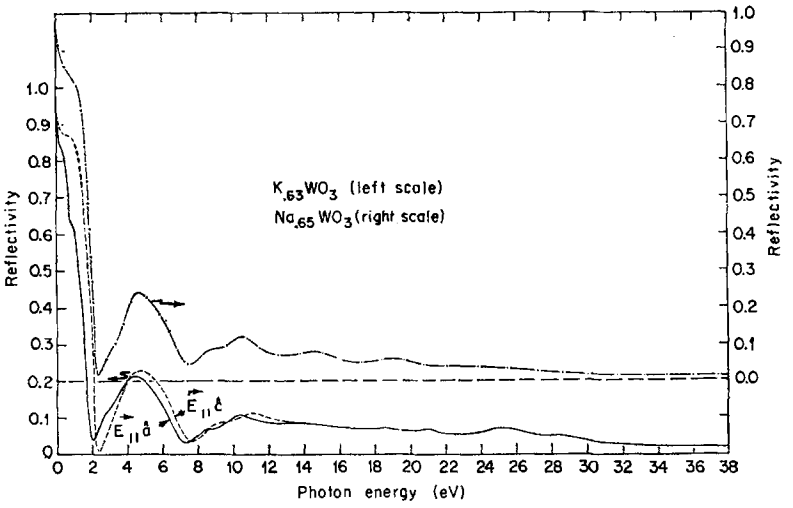

FIG. 3. Reflectivity of cubic $Na_{.65}WO_3$ [(—·) right scale] and tetragonal $K_{.63}WO_3$ at 300 K. (The data below 4.5 eV were taken at 4.2 K.)

shoulder at 19 eV although it could be related to the structures at 18.5 and 21 eV of $K_{.63}WO_3$. The Na bronze has a slight drop off at 25.5 eV, beyond which no further structure is seen. The reflectivity is 0.0115 at 38 eV.

A comparison of our $Na_{.65}WO_3$ data with the unpublished data of Feinleib and Scouler shows good agreement in the vuv to about 17 eV. There is excellent agreement with respect to the positions and relative magnitudes of the reflectivity structures although the measured magnitudes of our data are lower than those of Feinleib and Scouler, perhaps because of the near-absence of scattered light in our apparatus (24).

A comparison of the results shown in Figs. 1 and 2 with those of previous studies (*15*, *22*) on ReO_3 reveals considerable differences. While the crystal structure of the material is similar and the corresponding optical properties are expected to be similar, it is seen that the structure due to low energy interband transitions observed in ReO_3 (*22*) are not present in Na_xWO_3 or for $\mathbf{E}_{\parallel}\hat{c}$ in K_xWO_3. The only observed infrared structure was found for $\mathbf{E}_{\parallel}\hat{a}$ at about 0.9 eV while for

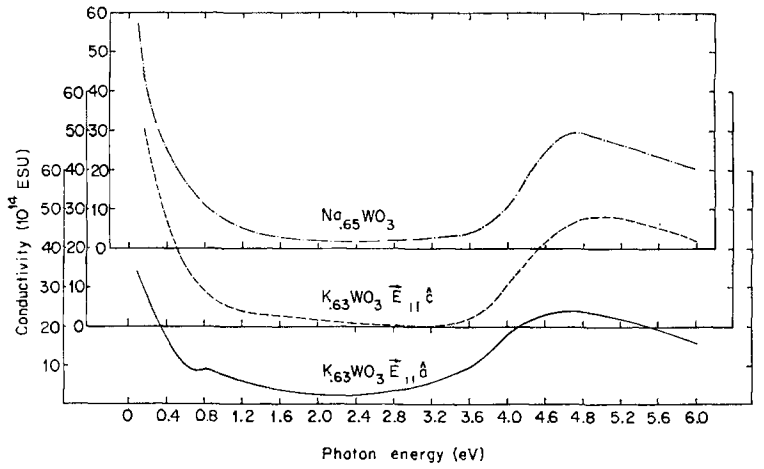

FIG. 4. Conductivity of $Na_{.65}WO_3$ and tetragonal $K_{.63}WO_3$ derived from the data in Fig. 3 by Kramers-Kronig analysis.

ReO_3 we reported structure at 0.4 and 1.0 eV (*22*). A comparison of the visible and vuv reflectivities reported here with those of ReO_3 of Feinleib, Scouler, and Ferretti (*15*) and Ref. (*22*) reveals the following:

1. The infrared features are quite different though the sharp rise in *A* to the peak at 2.3 eV for ReO_3 is practically identical to that of the Na bronzes.

2. The broad peak at about 4.5 eV also appears in ReO_3 although it drops off more rapidly on the high energy side in ReO_3.

3. The structures noted between 8 and 12 eV appear in ReO_3 but they may have been shifted to lower energy by slightly more than 1 eV; nonetheless, the peak occurs at nearly the same places for the bronzes, about 10.3 eV.

4. ReO_3 has a broad hump at about 14.5 eV which has a counterpart in the Na bronze and probably a weak counterpart at 14 eV for the K bronzes.

To Kramers-Kronig (KK) analyze our data we assumed free electron behavior below 0.1 eV. On the high energy side, another extrapolation was used which took the reflectivity smoothly to 0.1% at 1000 eV. It was assumed that there was no structure beyond the measured range. No corrections were made for a surface layer of any sort.

The phase of $\tilde{r}$ (Eq. 3) was calculated from *R* via the KK analysis (*5*) and from that and *R* it was possible to determine the optical constants. In Fig. 4 we display the calculated conductivity σ ($\sigma = \omega\varepsilon_2/4\pi = nkv$, where v is the frequency) for the Na and K bronzes for the energy range 0.1 to 6 eV. As expected, no interband absorption is apparent from the figure for Na_xWO_3 for $\mathbf{E}_\parallel \hat{c}$, while for $\mathbf{E}_\parallel \hat{a}$ a shoulder does appear at about 0.86 eV. All three curves share the common characteristic of dropping from a positive value (intraband absorption) to nearly zero, marking the onset of interband transitions. The minima occur at 2.28, 3.12, and 2.20 eV for $Na_{.65}WO_3$, $\mathbf{E}_\parallel \hat{c}$, and $\mathbf{E}_\parallel \hat{a}$, respectively. At higher energies, interband effects dominate.

The real part of the dielectric function, ε_1, rises from a large negative value, crosses the axis at the observed plasma energy (1.7, 2.05, and 2.05 eV for $\mathbf{E}_\parallel \hat{a}$, $\mathbf{E}_\parallel \hat{c}$ in $K_{.63}WO_3$, and $Na_{.65}WO_3$) and climbs to a large positive value with a peak at 3.8, 4.0, and 4.1 eV, respectively (not shown).

Figure 5 displays the imaginary part of the dielectric function, ε_2. The energy loss function is given by $\mathrm{Im}(-1/\tilde{\varepsilon}) = \varepsilon_2/(\varepsilon_1^2 + \varepsilon_2^2)$ and is shown in Fig. 6. The loss function is proportional to the probability that a fast electron will lose energy *E* in passing through the material (*5*, *28*). The dominant feature of each curve is a sharp spike occurring near 2.0 eV. It can be noted that for $\mathbf{E}_\parallel \hat{c}$ the spike is larger and has a smaller half-width than for either Na_xWO_3 or $\mathbf{E}_\parallel \hat{a}$, the latter having the broadest and shortest appearance. This peak is safely identified as a plasma resonance since ε_1 goes through zero, ε_2 is small,

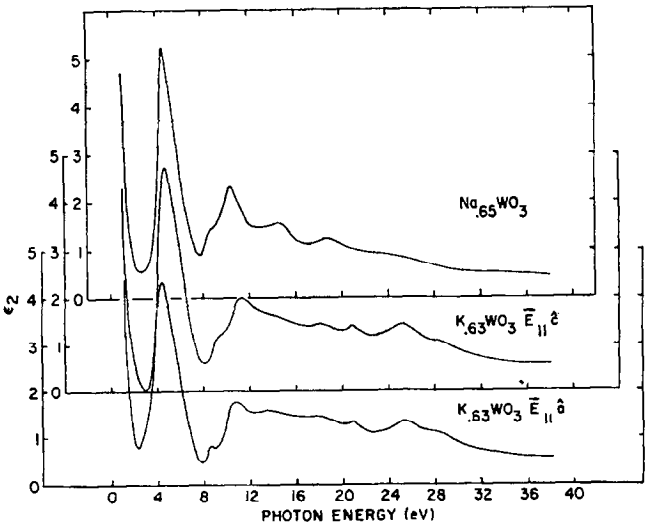

FIG. 5. Imaginary part of the dielectric constant of cubic $Na_{.65}WO_3$ and tetragonal $K_{.63}WO_3$ derived from the data in Fig. 3 by Kramers-Kronig analysis.

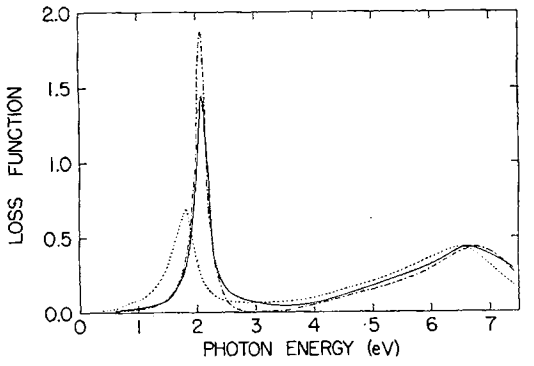

FIG. 6. Electron energy loss function, $\mathrm{Im}(-1/\varepsilon) = \varepsilon_2/(\varepsilon_1^2 + \varepsilon_2^2)$, for $Na_{.65}WO_3$ and tetragonal $K_{.63}WO_3$. (—) $Na_{.65}WO_3$; (---) $K_{.63}WO_3$, $E_{\parallel}\hat{a}$; (—·) $K_{.63}WO_3$, $E_{\parallel}\hat{c}$.

$d\varepsilon_2/dE < 0$, and $d\varepsilon_1/dE > 0$ (*28*). The second peak at 6.5 eV can probably also be identified as plasmon in origin, since it meets the above criteria. It appears that the higher energy structures in the loss function (not shown) all correspond to structure in ε_2 and are probably due to interband transitions.

Discussion

With the exception of exciton effects, the interband optical absorption of solids has been interpreted with impressive success by a quantum-mechanical one-electron model in which electric dipole transitions occur between occupied initial states $\Psi_i(\mathbf{k})$ with energy E_i and empty final states $\Psi_f(\mathbf{k})$ with energy E_f. In such transitions the wave vector $\mathbf{k}$ is conserved, so the transitions appear vertical on a band diagram such as Fig. 7. The contribution to ε_2 from interband transitions is

$$\varepsilon_2(\omega) = \frac{\hbar^2 e^2}{\pi m^2}\frac{1}{\omega^2}\int d^3k\,|\hat{e}\cdot\mathbf{p}_{if}|^2\,\delta(E_i - E_f - \hbar\omega), \tag{8}$$

where

$$\mathbf{p}_{if} = \int \Psi_f \mathbf{p} \Psi_i d^3r,$$

and $\hat{e}$ is the unit polarization vector of the light wave. Selection rules based on the symmetry of the wave vector $\mathbf{k}$ of the Bloch states forbid some transitions, and only allowed transitions will be discussed. If $\mathbf{p}_{if}$ is assumed not to depend much on energy, Eq. (8) simplifies to

$$\varepsilon_2(\omega) = \frac{\hbar^2 e^2}{\pi m^2}\frac{1}{\omega^2}|\hat{e}\cdot\mathbf{p}_{if}|^2\int\frac{ds}{|\nabla_k(E_f - E_i)|}, \tag{9}$$

where the integral is over a surface in $\mathbf{k}$-space on which $E_f - E_i = \hbar\omega$. This integral is often termed the joint density of states (JDOS), neglecting the constants involved. Structure in ε_2 arises either from small regions in $\mathbf{k}$-space for which the denominator in Eq. (9) vanishes

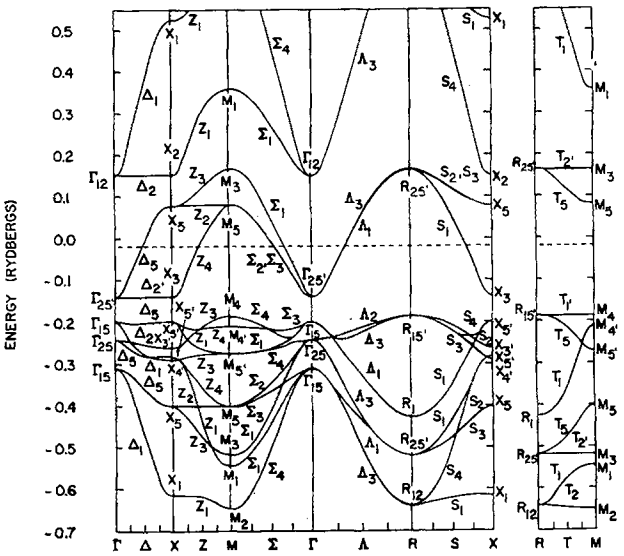

FIG. 7. Band structure of ReO_3 as calculated by Mattheiss [Ref. (*21*)].

(critical points in the joint density of states) as in insulators and semiconductors, or from large regions in **k** space where the denominator is small, as is common in metals. The former regions occur at symmetry points and lines, while the latter may occur throughout the Brillouin zone. Lacking detailed calculations, we discuss transitions along symmetry lines, but we have in mind larger volumes of **k** space, possibly near symmetry lines.

As mentioned earlier, it is probably the case that for Na_xWO_3 and for $\mathbf{E}_\parallel \hat{c}$ K_xWO_3, low energy interband transitions occur, but provide no structural features in the spectra. This is apparent from Figs. 1 and 2 which reveal only a smooth rise in A with no structure of any sort. When KK analyzed, the resulting ε_2 displays a characteristic free electron drop from a large positive value at low energies to nearly zero before the onset of interband effects, but the parameters so obtained for the free electron gas are erroneous because of the unresolved interband effects. This is not true for the $\mathbf{E}_\parallel \hat{a}$, however, since there is clearly structure in the absorptivity near 0.9 eV and hence in ε_2 at about 0.86 eV. Since no band structure calculations currently exist for the bronzes, it is difficult to identify the origin of this structure in more than a qualitative manner. In Fig. 7 we show the band structure of ReO_3 as calculated by Mattheiss (*21*) without spin–orbit effects. Because of the similarity between the materials, it appears reasonable to assume that the band structures are roughly similar. For all (cubic) Na bronzes, the total number of electrons per unit volume is slightly less than for ReO_3; this would lower the Fermi energy and affect the geometry of the Fermi surface.

In ReO_3 interband transitions were found at about 0.4 and 1.0 eV (*22*). The degenerate Σ_2, Σ_3 bands of Fig. 7 were known to be split by spin–orbit effects into nearly parallel Σ_5 bands. The 0.4 eV structure was attributed to transitions between these bands along Σ and in nearby regions of **k** space. The 1.0 eV feature was attributed to similar nearly parallel bands split by the crystal potential, $\Sigma_2, \Sigma_3 \rightarrow \Sigma_1$ ($\Sigma_5 \rightarrow \Sigma_5$ in double-group notation), also cut by the Fermi level. Similar bands should pertain to the cubic bronzes, with similar gaps. The fact that no such transitions are seen probably indicates a shift of the Fermi level from that of ReO_3 which could arise from small changes in the bands. If the Fermi level shifts up or down more than 0.5 eV (with respect to Γ'_{25}), the transitions would be shifted to sufficiently higher or lower energy as to be undetected in our data. Lesser shifts could reduce the matrix elements or the joint density of states enough to remove the salient structures of these transitions. An interband transition appears at 0.9 eV in the tetragonal $K_{.63}WO_3$, but only for $\mathbf{E}_\parallel \hat{a}$. Of the 12 equivalent Σ axes in a cubic crystal, only 4 remain in a tetragonal crystal, those in its basal plane. $\Sigma_5 \rightarrow \Sigma_5$ transitions are allowed for $\mathbf{E}_\parallel \hat{a}$ but not for $\mathbf{E}_\parallel \hat{c}$. This fits with what is observed, provided the Fermi level once again cuts the parallel bands, and the bands are similar to those in cubic ReO_3. However, this crystal has the tetragonal I structure of the tungsten bronze system, which is quite anisotropic (*29*). Those electrons propagating with **k** along the $\hat{c}$ axis see WO_6 octahedrons similar to those of cubic bronzes, but not connected to each other the same way. When **k** is perpendicular to the $\hat{c}$ axis, the charge density and hence the potential does not resemble that of a cubic bronze, even though there are still four Σ axes. Thus a detailed band structure is needed to see if there is any connection between the transitions in ReO_3 near 1.0 eV and those in $K_{.63}WO_3$ at 0.9 eV. At present, any connection seems tenuous. The anisotropy in the mobility of a tetragonal I sodium tungsten bronze was demonstrated by Muhlestein and Danielson (*30*). The mobility parallel to the $\hat{c}$ axis was similar to that of cubic bronzes, but the mobility normal to the $\hat{c}$ axis was not. This is qualitatively similar to what appears in the optical conductivity and is reasonable from structural considerations.

From Fig. 5 one can identify strong interband transitions as occurring at about 4.6 eV for all polarizations and samples. In the band scheme of Fig. 7, it is easy to identify possible contributants to this structure; this assumes that the bands have not beem drastically distorted. The bands Δ_2, Δ_2' are nearly parallel and give rise to a large joint density of states [see Eq. (9)]. This appears to be true also for Z_4 and Z_1, Σ_2, Σ_3, and Σ_1 as well as near Γ'_{25}, Γ_{12}. It is noted that $E(\Delta_2') - E(\Delta_2) \simeq 4$ eV. To the extent that the ReO_3 bands are applicable to the bronzes, then, we can account for the dominant structure in ε_2. The higher energy structure could likewise be tentatively identified but it seems more reasonable to present simply the ε_2 data and wait for a proper band calculation to be performed; such calculations would of course use the ε_2 data in the fitting of theory to experiment.

The plasma edge associated with the absorptivity peak near 2 eV has been discussed by Feinleib, Scouler, and Ferretti (*15*) for ReO_3. From Fig. 6, it is seen that the resonance in the tetragonal K bronze is the sharpest for $\mathbf{E}_\parallel \hat{c}$; the effect of the infrared interband transitions is seen to broaden and weaken the plasma resonance for $\mathbf{E}_\parallel \hat{a}$. From Fig. 5, we can see that the magnitude of ε_2 is practically zero for $\mathbf{E}_\parallel \hat{c}$—considerably smaller than for $\mathbf{E}_\parallel \hat{a}$ with a corresponding reduction in damping and a sharper, narrower loss function.

The peak in the loss function near 6.6 eV can be identified as a plasma resonance as pointed out in Ref. (*15*). The origin of higher energy structures in the loss function (not shown) can probably be attributed to structure in ε_2—all peaks in it correspond to structure in ε_2.

The dip on the high side of the reflectivity curves of Fig. 3 was identified by Consadori and Stella (*12*) as marking the onset of interband transitions. We have found that under KK analysis, the other mechanisms discussed above overwhelm any effect of interband transitions near 3.5 eV. There is no clear structure either in ε_2 or in the conductivity which can be clearly related to this R dip. Presumably, a broadening of the structure of Fig. 4 is a manifestation of such effects. It was observed (Figs. 2 and 3) that the dip in R is weakest for $\mathbf{E}_\parallel \hat{c}$. Were it stronger, one might observe a slightly larger value of the conductivity near 3.4 eV of $\mathbf{E}_\parallel \hat{c}$.

Interband transitions originating at core levels are well known. Those originating at s-levels are usually weak and Auger-broadened, making them difficult to detect. Of this type the potassium M_1–E_F transitions at about 33.9 eV and the oxygen L_1–E_F at 23.7 eV (*31*). [These energies are approximate and were taken from Ref. (*31*).] Those originating at p-levels are usually much stronger. In our energy range we expect sodium $L_{2,3}$–E_F (31.1 eV) and potassium $M_{2,3}$–E_F (17.8 eV). Referring to Fig. 5, the peak at 21.0 eV in $K_{.63}WO_3$, present in both polarizations, could arise from transitions of potassium $M_{2,3}$ electrons. The displacement of about 3 eV to higher energy could arise from a low density of states at E_F or matrix element effects. The following structures at 25.2 and 26.8 eV also could involve these core electrons. There is no detectable anisotropy in these structures. The corresponding sodium $L_{2,3}$–E_F transitions could correspondingly be shifted to about 34 eV and not be detected.

Conclusion

We have presented reflectivity spectra for samples of Na_xWO_3 and K_xWO_3 over the range 0.1 to 38 eV. The optical constants were then calculated and some tentative identifications of some of the structures have been made based upon band calculations of ReO_3. More definite identifications and interpretations of the structure must wait for better theoretical work with the bronzes. The data presented here should be useful in such calculations.

Acknowledgments

The authors thank H. R. Shanks for providing the crystals used in this study and for many informative conversations. Communication with Dr. W. Scouler is gratefully acknowledged. We thank the staff of the storage ring for their cooperation, especially E. M. Rowe, C. H. Pruett, and R. Otte. The storage ring is supported by the U.S. Air Force Office of Scientific Research.

References

1. H. R. Shanks, private communication.
2. A. Magnéli and B. Blomberg, *Acta Chem. Scand.* **5**, 372 (1951).
3. H. R. Shanks, P. H. Sidles, and G. C. Danielson, *Advan. Chem.* **39**, 237 (1963).
4. B. W. Brown and E. Banks, *J. Amer. Chem. Soc.* **76**, 963 (1954).
5. F. Stern, *Solid State Phys.* **15**, 299 (1963).
6. R. G. Dorothy and D. W. Lynch, unpublished data.
7. J. Feinleib and W. J. Scouler, unpublished data.
8. D. G. Avery, *Proc. Phys. Soc. London, Sect. B* **65**, 425 (1952).
9. P. G. Dickens, R. M. P. Quilliam, and M. S. Whittingham, *Mater. Res. Bull.* **3**, 941 (1968).
10. G. H. Taylor, *J. Solid State Chem.* **1**, 359 (1969).
11. S. Fujieda, *Sci. Light (Tokyo)* **18**, 1 (1969).
12. F. Consadori and A. Stella, *Lett. Nuovo Cimento* **3**, 600 (1970).
13. G. Giuliani, A. Gustinetti, and A. Stella, *Phys. Lett. A* **38**, 515 (1972).
14. T. Iwai, *J. Phys. Soc. Jap.* **15**, 1596 (1960)
15. J. Feinleib, W. J. Scouler, and A. Ferretti, *Phys. Rev.* **165**, 765 (1968).
16. J. B. Goodenough, *Bull. Soc. Chim. Fr.* 1200 (1965).
17. L. F. Mattheiss, *Phys. Rev. B* **2**, 3918 (1970).
18. W. R. Gardner and G. C. Danielson, *Phys. Rev.* **93**, 46 (1954).
19. M. E. Straumanis, *J. Amer. Chem. Soc.* **71**, 679 (1949).
20. E. W. Brimm, J. C. Brantley, J. H. Lorenz, and M. H. Jellinek, *J. Amer. Chem. Soc.* **73**, 5427 (1951).
21. L. F. Mattheiss, *Phys. Rev.* **181**, 987 (1969).
22. H. H. Weaver and D. W. Lynch, *Phys. Rev. B* **6**, 3620 (1972).

23. L. W. Bos AND D. W. LYNCH, *Phys. Rev. B* **2**, 4567 (1970).
24. C. G. OLSON AND D. W. LYNCH, unpublished data.
25. P. L. HARTMAN AND E. LOGOTHETIS, *Appl. Opt.* **3**, 255 (1964).
26. R. P. GODWIN, *Springer Tracts Mod. Phys.* **51**, 1 (1969), and references therein.
27. H. SHANKS, *J. Cryst. Growth* **13/14**, 433 (1972).
28. H. RAETHER, *Springer Tracts Mod. Phys.* **38**, 84 (1965).
29. A. MAGNÉLI, *Ark. Kemi* **1**, 213 (1949).
30. L. D. MUHLESTEIN AND G. C. DANIELSON, *Phys. Rev.* **158**, 825 (1962).
31. J. A. BEARDEN AND A. F. BURR, *Rev. Mod. Phys.* **39**, 125 (1967).